Structural and electrical properties of trimethylboron-doped silicon nanowires

Kok-Keong Lew, Ling Pan, Timothy E. Bogart, Sarah M. Dilts, Elizabeth C. Dickey, and Joan M. Redwing[a)]
Department of Materials Science and Engineering, Materials Research Institute, The Pennsylvania State University, University Park, Pennsylvania 16802

Yanfeng Wang, Marco Cabassi, and Theresa S. Mayer
Department of Electrical Engineering, The Pennsylvania State University, University Park, Pennsylvania 16802.

Steven W. Novak
Evans East, East Windsor, New Jersey 08520

(Received 16 April 2004; accepted 23 July 2004)

Trimethylboron (TMB) was investigated as a *p*-type dopant source for the vapor–liquid–solid growth of boron-doped silicon nanowires (SiNWs). The boron concentration in the nanowires was measured using secondary ion mass spectrometry and results were compared for boron-doping using TMB and diborane (B_2H_6) sources. Boron concentrations ranging from 1×10^{18} to 4×10^{19} cm^{-3} were obtained by varying the inlet dopant/SiH_4 gas ratio. TEM characterization revealed that the B_2H_6-doped SiNWs consisted of a crystalline core with a thick amorphous Si coating, while the TMB-doped SiNWs were predominantly single crystal even at high boron concentrations. The difference in structural properties was attributed to the higher thermal stability and reduced reactivity of TMB compared to B_2H_6. Four-point resistivity and gate-dependent conductance measurements were used to confirm *p*-type conductivity in the TMB-doped nanowires and to investigate the effect of dopant concentration on nanowire resistivity. © *2004 American Institute of Physics*. [DOI: 10.1063/1.1792800]

Silicon nanowires (SiNWs) are of interest for use as building blocks in the bottom-up assembly of nanoscale devices and circuits.[1,2] A number of prototype devices have been demonstrated including field effect transistors,[3] chemical and biological sensors,[4] and *p*–*n* junctions.[5] The ability to control the conductivity of the nanowires through intentional doping without unwanted changes in crystallinity is important for the realization of nanowire-based electronics.[3]

Vapor–liquid–solid (VLS) growth is the most common method used for the synthesis of SiNWs. In this technique, gold (Au) is used to catalyze the decomposition of a source gas, such as silane (SiH_4), resulting in the formation of a Au–Si liquid alloy provided that the temperature is greater than the eutectic temperature (~363 °C).[6,7] A single crystal SiNW is then precipitated from the liquid alloy when it becomes supersaturated with Si.[6,7] For boron-doped SiNWs, diborane (B_2H_6) has been used as a *p*-type dopant source in combination with SiH_4 during VLS growth.[8] However, prereaction between the two sources resulted in the deposition of a thick amorphous Si layer on the outer surface of the nanowire during growth. While this radial growth can be used to form *i*-Si/*p*-Si core-shell structures,[9] it is undesired for the fabrication of uniformly boron-doped nanowires. In this study, the use of trimethylboron [$(CH_3)_3B$ or TMB] has been investigated as an alternative *p*-type dopant source for SiNW growth due to its reduced reactivity compared to B_2H_6.

Anodized alumina membranes, with nominal pore diameters of 80 and 200 nm, were used as a platform for VLS growth of the boron-doped SiNWs, using a process similar to that reported previously.[10] VLS growth of boron-doped SiNWs was carried out in an isothermal quartz tube reactor at 500 °C with a total reactor pressure of 12 Torr using a 10% mixture of SiH_4 in H_2 as the source gas and either TMB (200 ppm in H_2) or B_2H_6 (100 ppm in H_2) as the dopant gas. The total gas flow rate was held constant at 100 sccm. The boron to silicon ratio in the inlet gas stream ($[B:Si]_{gas}$) was varied from 4.0×10^{-6} to 1.6×10^{-2} by changing the inlet gas flow rates of the dopant gas (TMB or B_2H_6) and SiH_4.

The nanowires were grown to a nominal length of 30 μm, such that they protruded approximately 25 μm out of the top surface of the membrane. All analyses were conducted on nominally undoped, TMB-doped, and B_2H_6-doped SiNWs to compare the doping efficiency of the two dopant sources. Secondary ion mass spectrometry (SIMS) was used to measure the boron concentration of the nanowires using a 3 keV O_2^+ beam. SIMS was carried out on the surface of membrane samples that contained a large collection of nanowires for boron detection. SiNWs were released from the membrane surface by mechanical agitation in an ultrasonic bath and suspended in isopropyl alcohol (IPA) for structural and electrical characterization.

The boron concentration of the intentionally doped SiNWs is plotted in Fig. 1 as a function of the B:Si inlet gas ratio. The boron concentration obtained in the nominally undoped nanowires ranged from approximately 1×10^{17} to 1×10^{18} cm^{-3}. These values represent the lower detection limit for boron in Si during the SIMS measurements. Consequently, it was difficult to accurately determine boron concentrations lower than $\sim1\times10^{18}$ cm^{-3} in the nanowires using SIMS analysis. In addition, it was not possible to compare residual carbon levels in nominally undoped, TMB

a)Author to whom correspondence should be addressed; electronic mail: jmr31@psu.edu

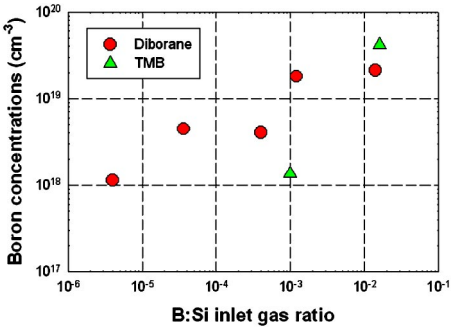

FIG. 1. (Color online) Boron concentration in SiNWs obtained by SIMS measurements as a function of the B:Si ratio in the inlet gas.

and B_2H_6-doped SiNWs using SIMS due to the effect of surface layer organic contaminants on the measurement. Boron concentrations ranging from 1×10^{18} to 4×10^{19} cm^{-3} were measured in the SiNWs doped with TMB demonstrating that this dopant source can be used for controlled boron incorporation.

Transmission electron microscopy (TEM) was used to characterize the structural properties of the nanowires. A suspension containing individual SiNWs was dropped onto lacey carbon grids. Experiments were conducted on a JEOL 2010F field-emission TEM (FE-TEM) operated at 200 kV. TEM micrographs of TMB-doped and B_2H_6-doped SiNWs that had similar boron concentrations ($2-4\times10^{19}$ cm^{-3}) are shown in Fig. 2. The majority of the TMB-doped SiNWs were found to be either single- or bi-crystalline, similar to that reported previously for nominally undoped nanowires.[11] As shown in Fig. 2(a), a representative TMB-doped SiNW is approximately 50 nm in diameter and single crystalline with a [111] growth direction and is covered by a thin 2 nm native oxide layer. In contrast, the representative B_2H_6-doped SiNW shown in Fig. 2(b) consisted of a crystalline Si core, approximately 30 nm in diameter, and an amorphous Si shell, approximately 30 nm thick, similar to that previously observed in B_2H_6-doped SiNWs.[9]

The different nanowire structures obtained with B_2H_6 and TMB can be explained by comparing the thermal stability and reactivity of the two sources with SiH_4. B_2H_6 in the gas phase decomposes at relatively low temperature forming monoborane (BH_3).[12] The B–B bond dissociation energy of B_2H_6 is approximately 27 kcal/mol.[12] Furthermore, B_2H_6 is known to react with SiH_4 leading to an increase in the Si growth rate for B_2H_6-doped films.[13–15] The increase in Si thin film deposition rate is believed to be responsible for the formation of the amorphous Si outer layer on the B_2H_6-doped nanowires. TMB decomposes via the sequential loss of methyl group (CH_3). The B–C bond dissociation energy in TMB is approximately 87 kcal/mol, leading to an increased thermal stability for TMB compared to B_2H_6.[16] The reduced reactivity of TMB enables the growth of highly B-doped SiNWs without a thick amorphous Si coating.

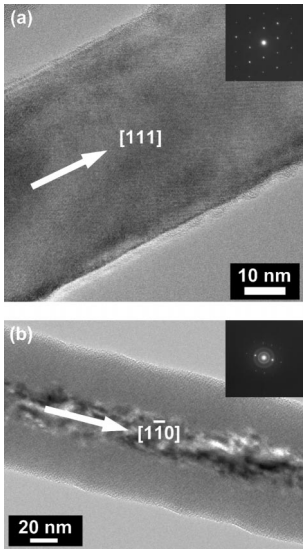

FIG. 2. HRTEM images of (a) TMB-doped ($[B:Si]_{gas}=1.6\times10^{-2}$) SiNW with [111] growth orientation. A thin oxide layer was observed on the outer surface. (b) B_2H_6-doped ($[B:Si]_{gas}=1.4\times10^{-2}$) SiNW consisting of a crystalline Si core surrounded by an amorphous Si shell.

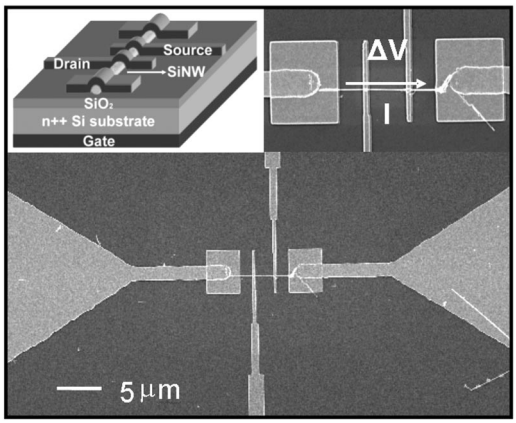

FIG. 3. FESEM image of the back-gated test structure used for four-point resistance and gate-dependent conductance measurements. A 3D schematic of the back-gated test structure is shown as an inset at the top left along with a high magnification image of the SiNW at the top right.

Four-point resistance and gate-dependent conductance measurements were carried out on nominally undoped, TMB-doped ($[B:Si]_{gas}=1.6\times10^{-2}$), and B_2H_6-doped ($[B:Si]_{gas}=1.4\times10^{-2}$) SiNWs with nominal 80 nm diameter to determine resistivity and doping type. Electrical characterization was conducted using a back-gated structure that includes four topside electrodes as shown in Fig. 3. The two internal electrodes serve as voltage probes for four-point resistance measurements and as drain (D) and source (S) electrodes for gate-dependent measurements. Samples were fabricated by integrating as-grown nanowires onto thermally oxidized n^{++}-Si substrates ($t_{ox}=160$ nm, $\rho\sim0.001$ Ω cm) by electrofluidic alignment[17] of individual SiNWs between pairs of lithographically defined electrodes. Topside electrodes were patterned in double-layer resist using electron-beam lithography (LEICA EBPG5-HR) followed by liftoff of Ti(80 nm)/Au(200 nm) deposited by thermal evaporation. The separation between the D/S electrodes varied from 1.6 to 3.2 μm for different devices on the test structure. All post-growth thermal treatment (e.g., contact anneal) was avoided to minimize unwanted impurity diffusion and activation that would make direct comparison of the as-grown SiNWs difficult.

Current–voltage characteristics measured between D/S electrodes separated by 2.2 μm for nominally undoped, TMB-, and B_2H_6-doped SiNWs are plotted in Fig. 4(a) and show that I_{DS} is linear and symmetric with V_{DS} for TMB- and B_2H_6-doped SiNWs. Variations in current of up to a factor of three were observed for different devices fabricated from the same growth run due to differences in wire diameter and

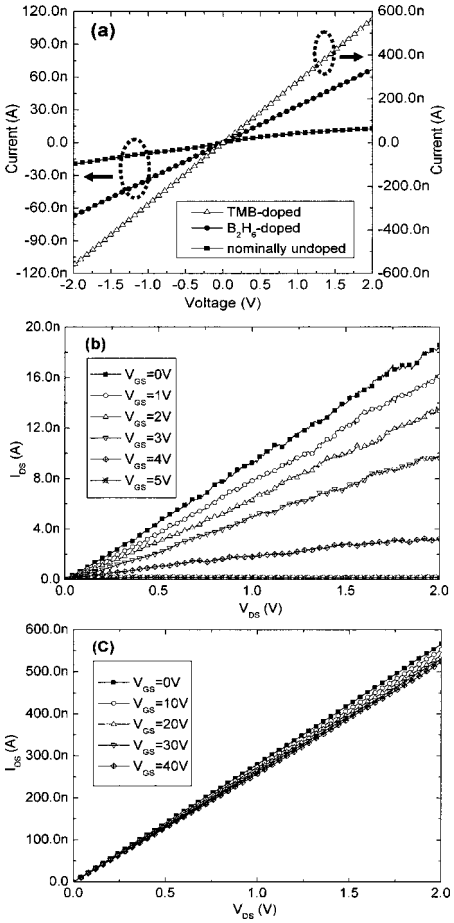

FIG. 4. (a) Two-point $I-V$ of nominally undoped, B_2H_6-doped (left current axis), and TMB-doped SiNWs (right current axis). Gate-dependent $I-V$ of the same (b) nominally undoped and (c) TMB-doped SiNW. The topmost curve in (b) and (c) plots are measured under $V_{GS}=0$ V. The gate voltage step for the nominally undoped SiNWs is $V_{GS}=+1$ V and that of the TMB-doped SiNWs is $V_{GS}=+10$ V.

contact resistance. The resistance of nominally undoped, TMB-doped, and B_2H_6-doped SiNWs found from the slope of these data sets is $R_T \sim 1\times10^8$, 3×10^6, and 2×10^7 Ω, respectively, which includes contributions due to nanowire and contact resistance. The SiNW resistance was isolated from contact resistance using the four-point configuration where the differential voltage ΔV developed across the two internal voltage probes was divided by the current forced between the two external electrodes. This gives resistances of $R_{\mathrm{SiNW}} \sim 3\times10^7$, 1×10^6, and 7×10^6 Ω, respectively, for the same SiNWs, and indicates that the contact resistance varies from $R_C \sim 1-35$ MΩ in these structures. Nanowire resistivity was determined from R_{SiNW} using dimensions measured by field-emission scanning electron microscopy (FESEM), and was found to be $\rho_{\mathrm{SiNW}} \sim 9.0$, 0.5, and 1.5 Ω-cm (see Fig. 3). The nanowire resistivity is higher than would be expected in bulk Si at similar acceptor concentrations. This may be the result of inaccuracies in the SIMS calibration, incorporation of compensating Au impurities during VLS growth,[18] or a reduction in hole mobility due to enhanced scattering. It should be noted that these values only provide an estimate of the nanowire resistivity because the effects of surface depletion or accumulation on the actual cross-sectional area responsible for conduction and the effect of the voltage probe contact barriers on channel potential are not taken into consideration. In addition, it is unlikely that the boron concentration in the SiNWs doped with B_2H_6 is uniform due to the presence of the thick amorphous shell structure. However, the trend to lower resistivity with the addition of TMB- or B_2H_6-dopant gases during VLS growth is consistent with the results of the SIMS analysis.

Gate-dependent I–V measurements of nominally undoped and TMB-doped SiNWs are plotted in Figs. 4(b) and 4(c). The nominally undoped SiNWs show a decrease in I_{DS} as V_{GS} is increased from $V_{GS}=0$ to the turn-off voltage of $V_{GS} \sim 5$ V. These characteristics are consistent with those expected for gate field modulation of the Schottky barrier formed between the S/D electrodes and SiNWs with *p*-type background concentration.[19] In comparison, the TMB-doped SiNWs have an I_{DS} that is approximately 30 times larger than the nominally undoped SiNWs at $V_{GS}=0$ V and smaller modulation of I_{DS} with increasing V_{GS}. These nanowires remain conductive for gate voltages as large as $V_{GS}=40$ V due to the heavier *p*-type doping and the relatively thick gate oxide. These gate-dependent I–V measurements further substantiate the SIMS and resistivity measurements, which indicate that boron is being incorporated into the SiNWs during synthesis.

In summary, *p*-type SiNWs have been successfully synthesized by using TMB as an alternative dopant source compared to B_2H_6. SIMS results demonstrated that incorporation of boron into SiNWs using TMB can be achieved and varied by changing the [B:Si] inlet gas ratio during VLS growth. Furthermore, high boron incorporation was not observed to alter the crystallinity of the SiNWs as occurs when B_2H_6 was used. Four-point resistivity and gate-dependent measurements confirm *p*-type conductivity in TMB-doped SiNWs.

This work was supported by the National Science Foundation (NSF) under Grant No. DMR-0103068 and The Pennsylvania State University Materials Research Science and Engineering Center (MRSEC) on Nanoscale Science.

[1] C. M. Lieber, Sci. Am. **285**, 59 (2001).
[2] Y. Cui, and C. M. Lieber, Science **291**, 851 (2001).
[3] Y. Cui, Z. Zhong, D. Wang, W. U. Wang, and C. M. Lieber, Nano Lett. **3**, 149 (2003).
[4] Y. Cui, Q. Wei, H. Park, and C. M. Lieber, Science **293**, 1289 (2001).
[5] M. S. Gudiksen, L. J. Lauhon, J. Wang, D. C. Smith, and C. M. Lieber, Nature (London) **415**, 617 (2002).
[6] R. S. Wagner and W. C. Ellis, Appl. Phys. Lett. **4**, 89 (1964).
[7] R. S. Wagner, W. C. Ellis, K. A. Jackson, and S. M. Arnold, J. Appl. Phys. **35**, 2993 (1964).
[8] Y. Cui, X. Duan, J. Hu, and C. M. Lieber, J. Phys. Chem. B **104**, 5213 (2000).
[9] L. J. Lauhon, M. S. Gudiksen, D. Wang, and C. M. Lieber, Nature (London) **420**, 57 (2002).
[10] K.-K. Lew, C. Reuther, A. H. Carim, and J. M. Redwing, J. Vac. Sci. Technol. B **20**, 389 (2002).
[11] A. H. Carim, K.-K. Lew, and J. M. Redwing, Adv. Mater. (Weinheim, Ger.) **13**, 1489 (2001).
[12] J. K. Bragg, L. V. McCarty, and F. J. Norton, J. Am. Chem. Soc. **73**, 2134 (1951).
[13] F. C. Eversteyn and B. H. Put, J. Electrochem. Soc. **120**, 106 (1973).
[14] C. M. Maritan, L. P. Berndt, N. G. Tarr, J. M. Bullerwell, and G. M. Jenkins, J. Electrochem. Soc. **135**, 1793 (1988).
[15] S. Nakayama, I. Kawashima, and J. Murota, J. Electrochem. Soc. **133**, 1721 (1986).
[16] H. Tarui, T. Matsuyama, S. Okamoto, H. Dohjoh, Y. Hishikawa, N. Nakamura, S. Tsuda, S. Nakano, M. Ohnishi, and Y. Kuwano, Jpn. J. Appl. Phys., Part 1 **28**, 2436 (1989).
[17] P. A. Smith, C. D. Nordquist, T. N. Jackson, T. S. Mayer, B. R. Martin, J. Mbindyo, and T. E. Mallouk, Appl. Phys. Lett. **77**, 1399 (2000).
[18] W. M. Bullis, Solid-State Electron. **9**, 143 (1966).
[19] J. Appenzeller, J. Knoch, V. Derycke, R. Martel, S. Wind, and Ph. Avouris, Phys. Rev. Lett. **89**, 126801 (2002).